Interval Methods for Sensitivity-Based Model-Predictive Control of Solid Oxide Fuel Cell Systems[*]

Andreas Rauh, Luise Senkel, Julia Kersten, Harald Aschemann

Chair of Mechatronics, University of Rostock,

Justus-von-Liebig-Weg 6, D-18059 Rostock, Germany

{Andreas.Rauh,Luise.Senkel,Julia.Kersten,Harald.Aschemann}@uni-rostock.de

Abstract

In control engineering, it is well known that model-predictive control approaches are characterized by inherent advantageous robustness and stability properties with respect to uncertainty in parameters and measured as well as estimated state variables. Therefore, the authors have developed interval-based extensions of model-predictive control procedures which allow for a direct consideration of bounded uncertainty during the computation of a robust control law. Moreover, it is directly possible to deal with state and input constraints. For that purpose, an implementation of the control procedure is necessary that can be evaluated in real time. This implementation makes use of interval analysis to determine state enclosures which describe guaranteed worst-case bounds of the reachable system states over a finite prediction horizon. In addition, the partial derivatives of state trajectories with respect to the manipulated variables involved in this procedure are determined efficiently by means of algorithmic differentiation. These derivatives are required to compute the control signal for both single-input single-output and multi-input multi-output systems. By means of the underlying state prediction procedure, it becomes possible to prevent with certainty the violation of both state and control constraints. A prototypical implementation of a corresponding control strategy is described in this paper. It is validated in simulation and experiment for the thermal subprocess of a high-temperature solid oxide fuel cell system.

---

1   Introduction

Control-oriented mathematical models for the thermal behavior of solid oxide fuel cell systems (SOFC systems) [13, 3, 27, 10, 28, 29, 6, 18] are characterized by the fact that internal parameters can only be determined within certain intervals [25, 7, 24]. This is caused by simplifications which are necessary to make mathematical system models usable for the synthesis of control strategies such that they can be evaluated in real time. Furthermore, temperature uncertainty due to limited measurement facilities in the interior of a fuel cell stack module (consisting of several individual cells which typically are installed in an electric series connection) as well as limited knowledge about the spatial distribution of the electrochemical reaction processes can be expressed by interval parameters in a natural way. Finally, disturbances result from the variation of electrical load demands which are a priori unknown to the controller. To determine control strategies which prevent the violation of constraints on both the admissible maximum operating temperatures and the corresponding spatial variation rates, it is reasonable to derive control laws directly accounting for these sources of uncertainty.

The approaches considered for this purpose are model-predictive control [5, 4] and sensitivity-based state and parameter estimation [22, 17]. Both procedures can be extended by using interval analysis to obtain a verified and, therefore, robust implementation which directly accounts for uncertain variables with a bounded range [21, 20].

Model-predictive control approaches are well-known means to stabilize dynamic systems and to compute input signals online which allow for both the tracking of desired state trajectories and for disturbance compensation in stationary operating points. These control procedures, which can be implemented by means of algorithmic differentiation[1] [9, 2], are inherently robust and can, therefore, also compensate disturbances to some extent which are neglected during the derivation of the predictive control strategy.

In this contribution, different verified extensions are described for the design of model-predictive control strategies. These controllers are implemented by applying interval analysis in real time. The use of interval analysis supports the design of controllers which prevent the violation of predefined (one-sided) tolerance bounds for desired state trajectories under consideration of given limitations for the actuator operating range.

Like any other interval technique for the evaluation of dynamic system models, interval-based predictive control procedures suffer from overestimation due to multiple dependencies on identical interval variables as well as the wrapping effect. In the case of predictive control procedures, this overestimation may lead to control strategies which are more conservative than necessary. To detect overestimation in the interval evaluation of the predictive control procedure, physical conservation properties (derived on the basis of the first law of thermodynamics) can be exploited in an algebraic consistency test. This test can be evaluated in real time in parallel to the computation of the control law.

This paper is structured as follows. In Sec. 2, an overview of sensitivity-based procedures for the design of tracking controllers is given with extensions to system models with interval uncertainty. Sec. 3 gives a brief summary of the most important modeling aspects of the thermal behavior of SOFC systems. For this type of application, the implementation of interval-based predictive control procedures is described

---

[1]The term *algorithmic differentiation*, as used in [9], is widely understood as a synonym for *automatic differentiation*. Throughout this paper, only procedures are employed which make use of operator overloading for the computation of derivatives.

in Sec. 4 on the basis of the mathematical model for a test rig available at the Chair of Mechatronics at the University of Rostock. Furthermore, representative simulation results and an experimental validation are presented in this section. This paper concludes with a discussion of future work in Sec. 5 focusing on algorithmic improvements for both reliable control strategies that can be used in real time and the dual problem of sensitivity-based state and parameter estimation.

2 Tracking Controllers for Continuous-Time Dynamic Systems

In this paper, robust tracking control strategies are presented for finite-dimensional dynamic systems which are described by sets of ordinary differential equations (ODEs) in terms of the nonlinear state equations[2]

$$\dot{\mathbf{x}}(t) = \mathbf{f}((\mathbf{x}(t), \mathbf{p}, \mathbf{u}(t), t) \tag{1}$$

and the corresponding system outputs

$$\mathbf{y}(t) = \mathbf{h}(\mathbf{x}(t), \mathbf{u}(t)) \ . \tag{2}$$

These outputs may coincide with the measured outputs $\mathbf{y}_m(t)$. In (1), $\mathbf{p}$ is a vector of system parameters, while $\mathbf{u}(t)$ contains all system inputs.

If the system outputs are not directly measurable, the outputs $\mathbf{y}(t)$ have to be computed on the basis of online estimates for the state vector $\mathbf{x}(t)$. These estimates are determined by state observers as, for example, described in [16]. Commonly, it is also necessary to employ state observers in the case that the outputs $\mathbf{y}_m(t)$ are measured directly. Then, the observer provides information about all internal system states $\mathbf{x}(t)$ which are required for the implementation of a reliable control strategy.

Using information about internal system states and measured outputs, control strategies are designed in this paper in such a way that the actual system outputs follow the desired output trajectory $\mathbf{y}_d(t)$ with good accuracy, even in cases in which the system dynamics are influenced significantly by uncertainty and disturbances.

Furthermore, it is necessary that the designed control strategies prevent with certainty the violation of feasibility constraints which are given as (upper) bounds for the admissible system states and possible control inputs.

In addition to model-predictive control procedures, several other approaches exist for the control of nonlinear dynamic systems. First, if a dynamic system is differentially flat or if coordinate transformations can be found which allow for an exact input-output linearization of the dynamics by means of a nonlinear state feedback approach, it is possible to design linear tracking controllers in a straightforward way [8]. However, this design is commonly performed for a nonlinear system model with nominal parameters. Afterwards, the robustness of the resulting system design is typically validated by means of simulations before the controller is applied to a real-life process. As shown in [12], interval and other verified methods are applicable to evaluate the robustness of control systems. However, if it cannot be guaranteed by the offline simulation

---

[2]Throughout this paper, vectors are denoted by boldface small letters and matrices by uppercase bold letters to distinguish them from scalar variables. Moreover, intervals are denoted explicitly by square brackets, e.g., $[\mathbf{x}] = \left([x_1] \quad \dots \quad [x_n] \right)^T$ represents an interval vector with $[x_i] = [\underline{x}_i \ ; \ \overline{x}_i]$, $\underline{x}_i \leq x_i \leq \overline{x}_i$, $i = 1, \dots, n$.

using verified ODE solvers that feasibility constraints are not violated, this two-stage design procedure has to be repeated iteratively. Here, the problem of overestimation in the computation of guaranteed state enclosures using interval analysis can be quite severe since long time horizons might be necessary for the simulation. Moreover, the simulation results are usually only valid for one specific (vector-valued) reference trajectory $\mathbf{y}_d(t)$.

Therefore, design procedures which use Lyapunov functions for an online stability analysis or for an online control design, respectively, are advantageous. These procedures can be determined in such a way that nonlinearities and uncertainties are directly accounted for. The design of guaranteed stabilizing control strategies by means of Lyapunov functions can be performed on the basis of the sliding-mode control methodology. Although this procedure allows for a verified stabilization of the system dynamics by using a variable structure control law which compensates the influence of all uncertain terms in a guaranteed way, the degrees of freedom for control optimization are limited in this case. Such an optimization might aim at a minimization of control switchings (to reduce actuator wear) or at a reduction of the energy for the actuators to achieve the control goal.

An overview of interval extensions of sliding mode control [31, 30] can be found in [25, 15, 24]. An improved flexibility with respect to the solution of the before-mentioned optimization task can be obtained by means of the predictive control procedure described in this paper. This even holds in cases in which the system is subject to uncertainty resulting from an imperfect knowledge about internal parameters $\mathbf{p} \in \left[\underline{\mathbf{p}} \,;\, \overline{\mathbf{p}}\right]$ and from an imperfect reconstruction of the state variables $\mathbf{x}(t) \in [\underline{\mathbf{x}}(t) \,;\, \overline{\mathbf{x}(t)}]$. As it will be shown in the following, it is not necessary to transform the sets of state equations into any kind of canonical form (like nonlinear controller normal form, input-affine system representations or strict feedback form) as is necessary for many other nonlinear control techniques.

2.1 Derivation of the Fundamental Sensitivity-Based Predictive Control Procedure

As an alternative to the two-stage, sliding-mode-type control procedure described in [25, 15, 24], a sensitivity-based procedure can be implemented. It is based on the analysis of the sensitivity of the solution $\mathbf{x}(t)$ to the set of ODEs $\dot{\mathbf{x}}(t) = \mathbf{f}(\mathbf{x}(t), \xi)$ with respect to a time-invariant parameter vector $\xi \in \mathbb{R}^{n_\xi}$.

Defining the new state vectors

$$\mathbf{s}_i(t) := \frac{\partial \mathbf{x}(t)}{\partial \xi_i} \in \mathbb{R}^{n_x} \quad \text{for all} \quad i = 1, \ldots, n_\xi \;, \tag{3}$$

the sensitivity equations

$$\dot{\mathbf{s}}_i(t) = \frac{\partial \mathbf{f}(\mathbf{x}(t), \xi)}{\partial \mathbf{x}} \cdot \mathbf{s}_i(t) + \frac{\partial \mathbf{f}(\mathbf{x}(t), \xi)}{\partial \xi_i} \tag{4}$$

with the corresponding initial conditions

$$\mathbf{s}_i(0) = \frac{\partial \mathbf{x}(0, \mathbf{p})}{\partial \xi_i} \tag{5}$$

can be derived. In (5), the relation $\mathbf{s}_i(0) = \mathbf{0}$ holds if $\mathbf{x}(0)$ is independent of ξ_i.

Now, the control error

$$J = \sum_{\mu=\nu}^{\nu+N_p} \mathcal{D}\left(\mathbf{y}\left(t_\mu\right) - \mathbf{y}_d\left(t_\mu\right)\right) \tag{6}$$

between the actual and desired system outputs $\mathbf{y}\left(t\right)$ and $\mathbf{y}_d\left(t\right)$, respectively, is defined to achieve an accurate tracking of desired output trajectories. As shown in [21, 20], $\mathcal{D}$ is a continuously differentiable measure — usually either linear or quadratic — for the output error $\mathbf{y}\left(t_\mu\right) - \mathbf{y}_d\left(t_\mu\right)$. Typical examples can be found in Sec. 4. The minimization of J is performed over a finite horizon of N_p prediction steps in real time by means of an analytic representation of the output vector

$$\mathbf{y}\left(t\right) = \mathbf{h}\left(\mathbf{x}\left(t\right), \mathbf{u}\left(t\right)\right) \tag{7}$$

in terms of the states $\mathbf{x}\left(t\right)$ and the control signal $\mathbf{u}\left(t\right)$, which is assumed to be piecewise constant for $t_\nu \leq t < t_{\nu+1}$.

After computing the differential sensitivity of the tracking error J by using algorithmic differentiation according to

$$\frac{\partial J}{\partial \Delta \mathbf{u}_\nu} = \sum_{\mu=\nu}^{\nu+N_p} \left(\frac{\partial \mathcal{D}\left(\mathbf{h}\left(\mathbf{x}, \mathbf{u}\right) - \mathbf{y}_d\left(t_\mu\right)\right)}{\partial \mathbf{x}} \cdot \frac{\partial \mathbf{x}\left(t_\mu\right)}{\partial \Delta \mathbf{u}_\nu} + \frac{\partial \mathcal{D}\left(\mathbf{h}\left(\mathbf{x}, \mathbf{u}\right) - \mathbf{y}_d\left(t_\mu\right)\right)}{\partial \Delta \mathbf{u}_\nu} \right) \;, \tag{8}$$

with

$$\frac{\partial \mathbf{x}\left(t_{\nu-1}\right)}{\partial \Delta \mathbf{u}_\nu} = \mathbf{0} \;, \tag{9}$$

a piecewise constant control law $\mathbf{u}\left(t_\nu\right)$ can be defined as

$$\mathbf{u}\left(t_\nu\right) = \mathbf{u}\left(t_{\nu-1}\right) + \Delta \mathbf{u}_\nu \tag{10}$$

with

$$\Delta \mathbf{u}_\nu = -\left(\frac{\partial J}{\partial \Delta \mathbf{u}_\nu}\right)^+ \cdot J \;. \tag{11}$$

Here, $\mathbf{M}^+ := \left(\mathbf{M}^T \mathbf{M}\right)^{-1} \mathbf{M}^T$ denotes the left pseudo-inverse[3] of the matrix $\mathbf{M}$. In (8), the differential sensitivity of J is computed by means of algorithmic differentiation [9], where the derivatives $\frac{\partial \mathbf{x}\left(t_\mu\right)}{\partial \Delta \mathbf{u}_\nu}$ are determined by an evaluation of the ODEs (4) with a suitable discretization scheme and the input vector $\mathbf{u} = \mathbf{u}\left(t_{\nu-1}\right) + \Delta \mathbf{u}_\nu$, $\Delta \mathbf{u}_\nu = \mathbf{0}$. Additionally, the property $\frac{\partial \mathbf{x}\left(t_{\nu-1}\right)}{\partial \Delta \mathbf{u}_\nu} = \frac{\partial \mathbf{x}\left(t_\nu\right)}{\partial \Delta \mathbf{u}_\nu} = \mathbf{0}$ has to be taken into account during the sensitivity analysis to ensure causality of the control strategy.

Moreover, the Jacobians $\frac{\partial \mathbf{h}}{\partial \mathbf{x}}$ and $\frac{\partial \mathbf{h}}{\partial \Delta \mathbf{u}_\nu}$ in (8) are evaluated along the predicted state trajectories $\mathbf{x} = \mathbf{x}\left(t_\mu\right)$. During the algorithmic differentiation of J, the control variations $\Delta \mathbf{u}_\nu$ are interpreted in the same way as the time-invariant parameters ξ in (4). A summary of the basic building blocks of the sensitivity-based control procedure can be found in Fig. 1.

---

[3] The matrix $\mathbf{M}^T \mathbf{M}$ is guaranteed to have full rank for all applications in this paper. This property coincides with the fact that the considered dynamic system models are *controllable*. A numerical proof of controllability is given by the existence of the transformation into nonlinear controller canonical form that is described in detail in [24]. Note that a symbolic statement of the corresponding controllability matrix is not reasonable for $n_x > 1$ in the case of the following SOFC model due to the excessive length of the symbolic expressions. Note that controllability of (24) is obvious for $n_x = 1$ since $\frac{\partial f}{\partial \mathbf{u}_1} \neq \mathbf{0}$ holds in this case.
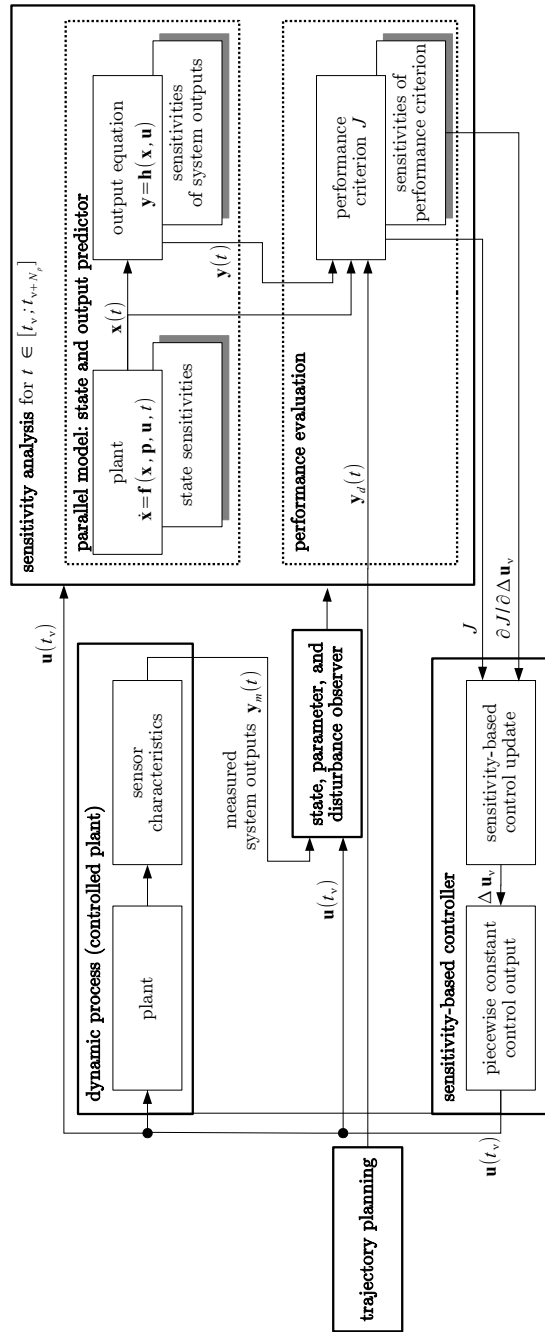
Figure 1: Fundamental sensitivity-based predictive control procedure.

2.2 Extension to Systems with Uncertainties

If interval uncertainties are taken into account for system parameters and measured outputs, the control signal can be computed after redefining the control increment $\Delta\mathbf{u}_\nu$ from (9) according to

$$\Delta\mathbf{u}_\nu = -\sup\left(\left(\frac{\partial[J]}{\partial\Delta\mathbf{u}_\nu}\right)^+ \cdot [J]\right) \ . \tag{12}$$

After evaluating the control law (10) with $\Delta\mathbf{u}_\nu$ defined in (12), the state equations are simulated by a suitable interval method (replacing the floating point method from the previous subsection) for the complete prediction horizon with the updated system input. This simulation leads to guaranteed enclosures of all reachable states over the corresponding horizon.

According to [21, 20], the updated input signal is applied to the real system for the time interval $[t_\nu \ ; \ t_{\nu+1}]$ if no violation of state constraints is detected over the time interval $\left[t_\nu \ ; \ t_{\nu+\tilde{N}_p}\right]$ with $\tilde{N}_p \leq N_p$. However, if a possible violation of state constraints is detected (here, overshooting maximum admissible state values), a further adjustment of the control input becomes necessary with

$$\Delta\tilde{\mathbf{u}}_\nu = -\sup\left(\left(\frac{\partial[\mathbf{y}]}{\partial\Delta\tilde{\mathbf{u}}_\nu}\right)^+ \cdot \overline{\Delta\mathbf{y}_\nu}\right) \tag{13}$$

and

$$\mathbf{u}(t_\nu) := \mathbf{u}(t_\nu) + \Delta\tilde{\mathbf{u}}_\nu \ . \tag{14}$$

In (13), the term $\overline{\Delta\mathbf{y}_\nu}$ is given as

$$\overline{\Delta\mathbf{y}_\nu} := \max_{t\in\left[t_\nu \ ; \ t_{\nu+\tilde{N}_p}\right]} \left\{0 \ , \ \sup\left([\mathbf{y}(t)] - \mathbf{y}_d(t)\right)\right\} \ , \tag{15}$$

where the operators *max* and *sup* are defined component-wise. It denotes the maximum possible overshoot of the desired trajectory over the prediction horizon.

A detailed discussion of this procedure — and an extension to path following in cases for which control constraints are violated — can be found in [21].

2.3 Illustrative Example

As a simple illustrative example, the design of a predictive controller is considered for the double integrating plant

$$\dot{\mathbf{x}}(t) = \begin{pmatrix} 0 & 1 \\ 0 & 0 \end{pmatrix} \mathbf{x}(t) + \begin{pmatrix} 0 \\ \frac{1}{m} \end{pmatrix} u(t) + \begin{pmatrix} 0 \\ a_d \end{pmatrix} \quad \text{with} \quad \mathbf{x}(t) = \begin{pmatrix} x_1(t) \\ x_2(t) \end{pmatrix} \ . \tag{16}$$

This system model corresponds to an accelerated mass m with the input force $u(t)$ and the additive disturbance a_d. Moreover, $x_1(t)$ denotes the position, and $x_2(t)$ denotes the velocity.

In (16), only conservative bounds are assumed to be known for the mass m and for the disturbance a_d (representing an acceleration error) during control synthesis. All following simulations are performed for the dimensionless parameter intervals $m \in [m] = [0.9 \ ; \ 1.1]$, and $a_d \in [a_d] = [-0.1 \ ; \ 0.1]$.

The goal of the design of a suitable controller is the tracking of the desired output trajectory defined by

$$y_d(t) = x_{1,d}(t) = 1 - e^{-t} \tag{17}$$

despite the inconsistent initial state vector $\mathbf{x}(0) = \begin{pmatrix} -1 & 0 \end{pmatrix}^T$.

Applying the fundamental sensitivity-based predictive control procedure (without the extension for overshoot prevention) leads to the results in Fig. 2. Here, the constant step size $t_{\nu+1} - t_\nu = 0.01$ with the prediction horizon $N_p = 200$ has been used in the evaluation of the sensitivity-based control scheme (8)–(10). The simulation results have been obtained by gridding each of the corresponding parameter intervals $[m]$ and $[a_d]$ into 10 equally spaced points.

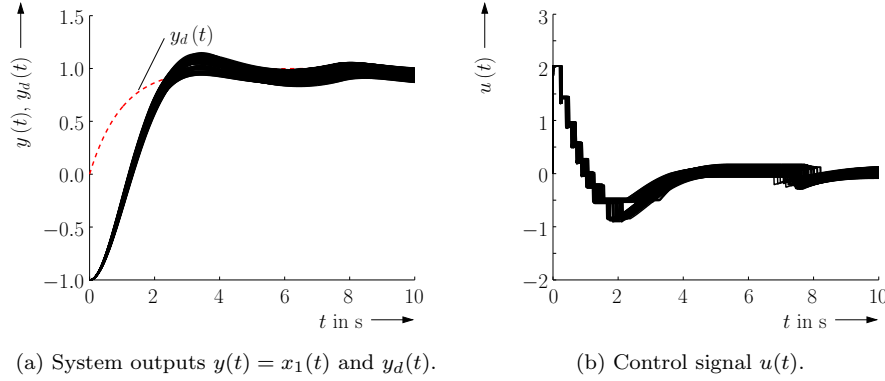(a) System outputs $y(t) = x_1(t)$ and $y_d(t)$.   (b) Control signal $u(t)$.

Figure 2: Fundamental sensitivity-based control procedure for the illustrative example with an interval-based evaluation of the performance criterion J.

Obviously, the fundamental control procedure is not able to prevent overshooting the desired trajectory $y_d(t)$. This can be avoided despite both the above-mentioned uncertainties and the bounded measurement errors

$$x_1(t) \in x_{1,m}(t) + [-0.01 \; ; \; 0.01] \quad \text{and} \quad x_2(t) \in x_{2,m}(t) + [-0.01 \; ; \; 0.01] \tag{18}$$

if the control law is evaluated by the extended definition (12), where (13) and (14) are used as additional corrections. In (18), the index m denotes the measured quantities provided by appropriate sensors. Then, the results shown in Fig. 3 are obtained. Further details about the choice of the performance criterion J can be found in [21].

To improve the convergence properties of the sensitivity-based control procedure, it is possible to introduce optional step size control factors $0 < \alpha_i < 1$, $i \in \{1, 2, 3\}$, in (11), (12), and (13) according to

$$\Delta \mathbf{u}_\nu = -\alpha_1 \cdot \left(\frac{\partial J}{\partial \Delta \mathbf{u}_\nu} \right)^+ \cdot J \; , \tag{19}$$

$$\Delta \mathbf{u}_\nu = -\alpha_2 \cdot \sup \left(\left(\frac{\partial [J]}{\partial \Delta \mathbf{u}_\nu} \right)^+ \cdot [J] \right) \; , \tag{20}$$

(a) System outputs $y(t) = x_1(t)$ and $y_d(t)$.

(b) Control signal $u(t)$.

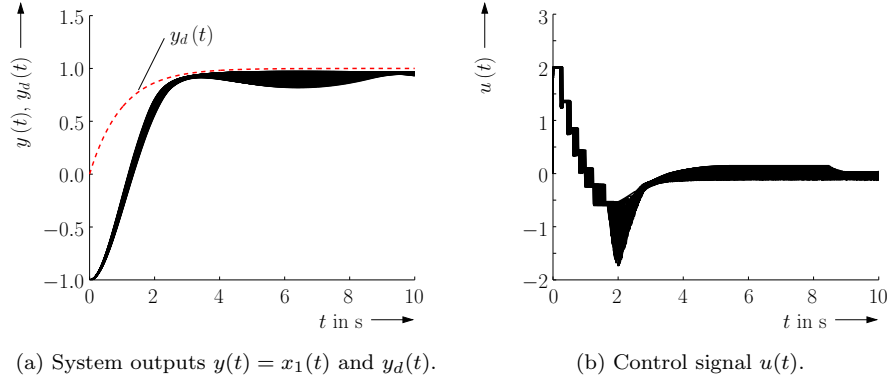Figure 3: Results of the extended sensitivity-based control procedure.

and

$$\Delta \tilde{\mathbf{u}}_\nu = -\alpha_3 \cdot \sup\left(\left(\frac{\partial [\mathbf{y}]}{\partial \Delta \tilde{\mathbf{u}}_\nu} \right)^+ \cdot \overline{\Delta \mathbf{y}_\nu} \right) \ . \tag{21}$$

3 Practical Application Scenario: Temperature Control for Solid Oxide Fuel Cell Systems

This section gives a brief overview of control-oriented modeling procedures for the thermal behavior of SOFC systems. The corresponding models are then used for the design of sensitivity-based control procedures which allow for disturbance compensation in stationary operating points as well as for trajectory tracking in the non-stationary heating phase of the system.

3.1 Control-Oriented Low-Order Model

To describe the thermal behavior of an SOFC with sufficient accuracy for control purposes, integral energy balances are necessary in the form of a finite volume model, given in terms of a coupled set of nonlinear ODEs. In these ODEs (a detailed derivation can be found in [3, 18, 19, 25]), the effects depicted in Fig. 4 are included: internal heat conduction and enthalpy flows of the anode gas (AG) and cathode gas (CG) with temperature-dependent heat capacities, exothermic reaction processes ($\dot{Q}_R$) with temperature-dependent reaction enthalpies, heat transfer between the stack module and the ambient medium ($\dot{Q}_A$), as well as heat production due to internal Ohmic losses (P_{El}).

The exothermic reaction between the fuel gas supplied to the anode (in this paper, pure hydrogen) and the cathode gas (air) results from the electrochemical reaction

$$2 \, H_2 + 2O^{2-} \rightarrow 2 \, H_2O + 4e^- \quad \text{and} \quad O_2 + 4e^- \rightarrow 2O^{2-} \tag{22}$$

taking place at the anode and cathode in the SOFC stack. To develop robust control strategies, it is essential to be able to cope with non-stationary operating points of the
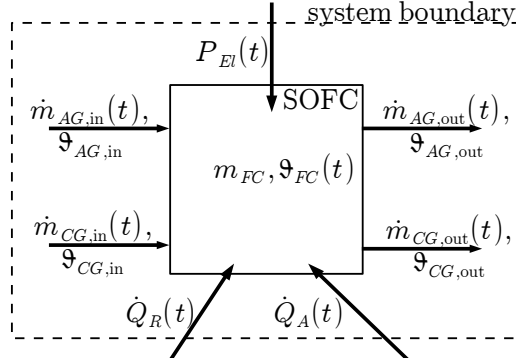
Figure 4: Integral energy balance for the SOFC stack module.

SOFC, in which the heat production due to the exothermic reaction (22) as well as the Ohmic losses in the interior of the stack module are not constant over time. This is caused by an a priori unknown variation of the demand for the electrical power to be supplied to a consumer.

To reduce thermal stress on the stack module materials, inevitably leading to an accelerated degradation of the cell materials, it is essential to keep the system temperature as close as possible to a desired set-point. Simultaneously, spatial gradients of the internal stack temperature have to be minimized effectively despite external disturbances.

For that reason, the temperature distribution in the SOFC stack is described in this paper by different finite volume models with user-defined spatial resolutions. The complexity of these models ranges from a global system model, which only provides one lumped temperature ϑ_{FC} for the complete SOFC system, to finite volume models in which the temperature distribution is described after a semi-discretization into $n_x = L \cdot M \cdot N > 1$ finite volume elements (cf. Fig. 5).

In Fig. 5, the variables L, M, and N represent the numbers of finite volume elements along each space coordinate, which can be chosen in a problem-oriented way. For each volume element (i, j, k), an integral energy balance

$$
\begin{aligned}
c_{i,j,k} m_{i,j,k} \dot{\vartheta}_{i,j,k}(t) = {} & C_{AG,i,j,k}(\vartheta, t) \cdot (\vartheta_{i,j-1,k}(t) - \vartheta_{i,j,k}(t)) \\
& + C_{CG,i,j,k}(\vartheta, t) \cdot (\vartheta_{i,j-1,k}(t) - \vartheta_{i,j,k}(t)) \\
& + \dot{Q}_{\eta,i,j,k}(t) + \dot{Q}_{R,i,j,k}(t) + P_{El,i,j,k}(t)
\end{aligned}
\tag{23}
$$

is set up according to the effects described above with the local specific heat capacity $c_{i,j,k}$ and the local mass parameter $m_{i,j,k}$. The expressions $C_{AG,i,j,k}(\vartheta, t)$ and $C_{CG,i,j,k}(\vartheta, t)$ depend on both gas temperatures as well as on their corresponding mass flows.

Under consideration of the inter-element conditions characterizing the continuity of the heat flow over each boundary surface between neighboring finite volume elements, a set of ODEs

$$
\dot{\mathbf{x}}(t) = \mathbf{f}\left(\mathbf{x}(t), \mathbf{p}, \mathbf{u}_1(t), \mathbf{u}_2(t)\right)
\tag{24}
$$

is obtained with the state vector $\mathbf{x}^T = \begin{pmatrix} \vartheta_{1,1,1} & \dots & \vartheta_{L,M,N} \end{pmatrix} \in \mathbb{R}^{n_x}$. The parameter vector $\mathbf{p}$ in (24) has been identified experimentally by the procedures described in [19,
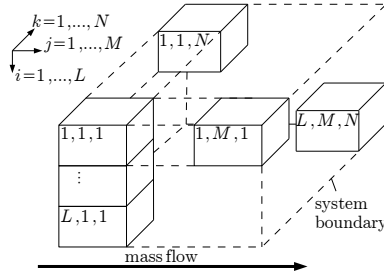
Figure 5: Semi-discretization of the fuel cell stack module into finite volume elements.

1]. Moreover, the control vector $\mathbf{u}_1$ consists of the mass flow $\dot{m}_{CG,in}$ of preheated cathode gas with the temperature $\vartheta_{CG,in}$. The vector $\mathbf{u}_2$ contains all other system inputs, which are the mass flows of hydrogen ($\dot{m}_{H_2}$), nitrogen ($\dot{m}_{N_2}$) and water vapor ($\dot{m}_{H_2O}$) at the anode with their temperature $\vartheta_{AG} = \vartheta_{AG,in}$ as well as the electric current

$$I = \sum_{i,j,k} I_{i,j,k} \quad , \tag{25}$$

see also (28).

In (23), the term

$$\dot{Q}_{\eta,i,j,k}(t) = \sum_{\eta \in \mathcal{N}} \frac{1}{R_{th,\eta}^{i,j,k}} \left(\vartheta_\eta(t) - \vartheta_{i,j,k}(t) \right) \tag{26}$$

characterizes the heat transfer and the heat conduction by the thermal resistance $R_{th,\eta}^{i,j,k}$ from all neighboring volume elements denoted by the multi-index $\eta \in \mathcal{N}$ to the volume element (i,j,k). In (26), the resistances for heat conduction in the interior of the semi-discretized fuel cell stack module are distinguished from thermal resistances for finite volume elements with a direct connection to the environment, leading to different values for the corresponding variables $R_{th,\eta}^{i,j,k}$ in the parameter identification. Here, the thermal resistances on the system boundary are typically larger due to the insulation layer than the ones in the interior of the fuel cell stack module which correspond to an averaged material parameter of the electrodes, the solid electrolytes, and the interconnection layers. The term $(\vartheta_\eta - \vartheta_{i,j,k})$ represents either the temperature difference to the neighboring finite volume elements in the interior of the stack or the temperature difference to the surrounding air. Here, the temperatures of the neighboring elements are denoted by ϑ_η, while ϑ_A is the ambient temperature.

The reaction enthalpy is included in the model (23) by the relation

$$\dot{Q}_{R,i,j,k}(t) = \frac{\Delta_R H_{i,j,k}(\vartheta_{i,j,k}) \cdot \dot{m}_{H_2,i,j,k}^R(t)}{M_{H_2}} \tag{27}$$

in terms of the local temperature-dependent molar reaction enthalpy $\Delta_R H_{i,j,k}(\vartheta_{i,j,k})$ and the local molar flow of hydrogen $\frac{\dot{m}_{H_2,i,j,k}^R}{M_{H_2}}$. Furthermore, Faraday's law for electrochemical reactions yields

$$\dot{Q}_{R,i,j,k}(t) = \Delta_R H_{i,j,k}(\vartheta_{i,j,k}) \frac{I_{i,j,k}(t)}{z\,F} \tag{28}$$

with the electric current $I_{i,j,k}$ in the corresponding volume element, the Faraday constant F, and the number of electrons z transferred in the overall reaction (22) [3]. The electric current $I_{i,j,k}$ significantly influences the local Ohmic losses $P_{El,i,j,k}(t) = R_{El,i,j,k} I_{i,j,k}^2(t)$ with the internal resistance $R_{El,i,j,k}$. For the computation of the heat capacities $C_{AG,i,j,k}(\vartheta_{i,j,k}, t)$ and $C_{CG,i,j,k}(\vartheta_{i,j,k}, t)$ of the fluids inside each finite volume element, the local consumption of hydrogen H_2 at the anode, of oxygen O_2 at the cathode, and the local production of water vapor H_2O at the anode have to be taken into account as described in [19].

3.2   Methods for Reduction of Overestimation

As mentioned in the previous section, the interval-based predictive control procedure uses an online evaluation of the state equations of the thermal SOFC model over the time horizon $t \in \left[t_\nu \; ; \; t_{\nu+N_p}\right]$ with $N_p > 0$ steps and a constant sampling time $T := t_{\nu+1} - t_\nu$. During this evaluation, overestimation arises due to multiple dependencies on common interval variables as well as due to the wrapping effect [11].

   This overestimation in the resulting state enclosures can make the predictive control procedure inefficient and unnecessarily conservative. Hence, the following energy-related criterion is used for an online detection and reduction of overestimation.

3.2.1   The Continuous-Time Case: General Formulation

Firstly, the energy-related term

$$E_\mu := E\left(t_\mu\right) = \sum_{i,j,k} c_{i,j,k} \cdot m_{i,j,k} \cdot \vartheta_{i,j,k}(t_\mu) \tag{29}$$

is evaluated directly for the predicted state intervals $\vartheta_{i,j,k}(t_\mu) \in [\vartheta_{i,j,k}(t_\mu)]$. These intervals already contain the overestimation due to both above-mentioned effects.

   Secondly, the physically equivalent integral formulation

$$E_\mu = E_\nu + \int_{t_\nu}^{t_\mu} \dot{E}\left(\tau\right) d\tau = E_\nu + \int_{t_\nu}^{t_\mu} \left(\sum_{i,j,k} c_{i,j,k} \cdot m_{i,j,k} \cdot \dot{\vartheta}_{i,j,k}(\tau) \right) d\tau \tag{30}$$

is computed. The variant (30) typically leads to tighter interval bounds than the variant (29) if it is evaluated for uncertain parameters $\mathbf{p} \in [\mathbf{p}]$ and for uncertain states $\vartheta_{i,j,k}(t_\nu) \in [\vartheta_{i,j,k}(t_\nu)]$. The reason for this property can be explained by the fact that the integrand in (30) can be simplified symbolically before the interval evaluation. Then, due to the first law of thermodynamics (describing the conservation of energy) common expressions cancel exactly which are related to the heat flows between directly neighboring finite volume elements. These terms are related to the heat conduction terms included in (26), which are the basic coupling terms between the individual components of the vector-valued function $\mathbf{f}$ in (24) and, therefore, also the source for overestimation in an interval-based computation of state enclosures over the time horizon $t \in \left[t_\nu \; ; \; t_{\nu+N_p}\right]$.

3.2.2   The Continuous-Time Case: Simplified Formulation

If the finite volume model for the thermal behavior of the SOFC is described with state-independent and time-invariant parameters $c_{i,j,k}$ and $m_{i,j,k}$ which are identical for all finite volume elements, the following simplifications become possible.

Equation (29) can be replaced with

$$E_\mu := E\left(t_\mu\right) = \sum_{i,j,k} \vartheta_{i,j,k}(t_\mu) \tag{31}$$

and equation (30) with the expression

$$E_\mu = E_\nu + \int\limits_{t_\nu}^{t_\mu} \dot{E}\left(\tau\right) d\tau = E_\nu + \int\limits_{t_\nu}^{t_\mu} \left(\sum_{i,j,k} \dot{\vartheta}_{i,j,k}(\tau)\right) d\tau \ . \tag{32}$$

In both (30) and (32), the offset $E_\nu \in [E_\nu] = [E(t_\nu)]$ is determined on the basis of measured temperatures including interval bounds for measurement tolerances and estimation errors at the point of time $t = t_\nu$.

3.2.3 The Discrete-Time Case

Both formulations above rely on a continuous-time system model. However, verified integration of the ODEs, characterizing the thermal behavior of the fuel cell, can be replaced with good accuracy by a pure discrete-time formulation in which the time discretization error is neglected. Due to sampling step sizes which are smaller by at least two orders of magnitude than the time constants of the system, the resulting errors have significantly less effect on the state enclosure than the uncertainties in parameters and measured state variables. Hence, the following *verified explicit Euler method* is used for all further evaluations.

The corresponding discrete-time approximation of the thermal subsystem of the SOFC, described by the state equations (24) for the complete prediction horizon $\left[t_\nu \ ; \ t_{\nu+N_p}\right]$, $\mu > \nu$, is replaced by

$$\vartheta_{i,j,k}\left(t_\mu\right) \in \left[\vartheta_{i,j,k}\left(t_{\mu-1}\right)\right] + T \cdot \left[\dot{\vartheta}_{i,j,k}\left(t_{\mu-1}\right)\right] \tag{33}$$

with the piecewise constant inputs $\mathbf{u}_1 = \mathbf{u}_1\left(t_{\nu-1}\right)$ and $\mathbf{u}_2 = \mathbf{u}_2\left(t_{\nu-1}\right)$.

In analogy to the continuous-time case described above, an energy-related criterion for the detection and reduction of overestimation at the point of time t_μ can be derived in the discrete formulation.

Then, the expression (31) is replaced by

$$E_\mu \in [E(t_\mu)] = \sum_{i,j,k} \left[\vartheta_{i,j,k}(t_\mu)\right] \tag{34}$$

and the term (32) — which is a simplified version of (30) — by its equivalent discrete-time term

$$E_\mu \in \left[\tilde{E}_\mu\right] := \left[\tilde{E}_\nu\right] + \sum_{\zeta=\nu}^{\mu} T \cdot \left(\sum_{i,j,k} \left[\dot{\vartheta}_{i,j,k}(t_\zeta)\right]\right) \ . \tag{35}$$

Here, t_ν is the starting point of the time horizon for which the performance criterion J for the predictive controller is evaluated.

Overestimation in the resulting state enclosures can be detected by the following consistency test: Firstly, the interval vector $[\mathbf{x}\left(t_\mu\right)]$ is subdivided into subintervals $[\mathbf{x}'\left(t_\mu\right)]$ along its longest edge. Then,

$$E'_\mu \in \left[E'_\mu\right] = \sum_{i,j,k} \left[\vartheta'_{i,j,k}(t_\mu)\right] \tag{36}$$

is evaluated for $[\mathbf{x}'(t_\mu)]$ according to (34):

- The subinterval $[\mathbf{x}'(t_\mu)]$ is guaranteed to be caused by overestimation if $\left[E'_\mu\right] \cap \left[\tilde{E}_\mu\right] = \emptyset$ holds.

- In the case $\left[E'_\mu\right] \subseteq \left[\tilde{E}_\mu\right]$, $\left[\tilde{E}_\mu\right]$ is consistent with (35).

- All further intervals, for which $\left[E'_\mu\right] \cap \left[\tilde{E}_\mu\right] \neq \emptyset$ and $\left[E'_\mu\right] \not\subseteq \left[\tilde{E}_\mu\right]$ hold, are undecided and can be examined after further subdivision.

The evaluation of $[J]$ is then again performed for the reduced predicted overshoot, see for example (15). All further update rules for the piecewise constant predictive control law remain unchanged.

4   Simulation and Experimental Validation

In this section, different variants for interval-based predictive control procedures are designed and compared by simulations and experiments with the following objectives:

1. The system inputs and operating temperature should stay close to their desired set-points.

2. Large spatial gradients of the temperature distribution in the interior of the SOFC stack module have to be penalized.

3. Local violations of a maximum admissible cell temperature should be prevented with good accuracy.

4. Temporal variation rates of the physical system inputs should be accounted for in a suitable, parameterizable cost function.

Besides a global system model, containing only a single temperature ϑ_{FC} ($L = 1$, $M = 1$, $N = 1$), the system model depicted in Fig. 6 is investigated. In both cases, a sensitivity-based manipulation of the supplied mass flow of cathode gas $\dot{m}_{CG}$ and its corresponding temperature ϑ_{CG} is used to determine the control input $\mathbf{u}_1$. All other inputs $\mathbf{u}_2$ are specified by independent underlying controllers that cannot be influenced by the choice of $\mathbf{u}_1$.
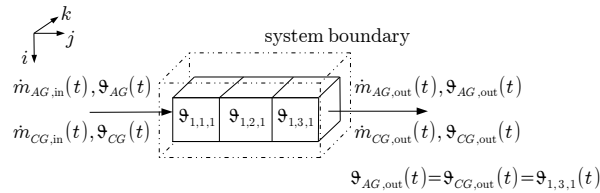

Figure 6: Semi-discretization of the stack module into three finite volume elements along the direction of the gas mass flow.

4.1   Comparison of Different Performance Criteria

In all following simulations and experiments, the inputs $\mathbf{u}_2$ are assumed to be uncertain over the prediction horizon ($N_p = 40$, $t_{\mu+1} - t_\mu = 1\,$s for all simulations) according to $\mathbf{u}_2 \in \text{diag}\,\{[0.95\;;\;1.05]\,,\dots,[0.95\;;\;1.05]\} \cdot \mathbf{u}_{2,m}$, where $\mathbf{u}_{2,m}$ is a vector containing input data gathered during one heating phase of the SOFC test rig, see Fig. 7. Moreover, the measured stack temperatures are assumed to be affected by the additive, independent measurement tolerances $[-2.5\;;\;2.5]$ K in each point of time $t = t_\nu$.
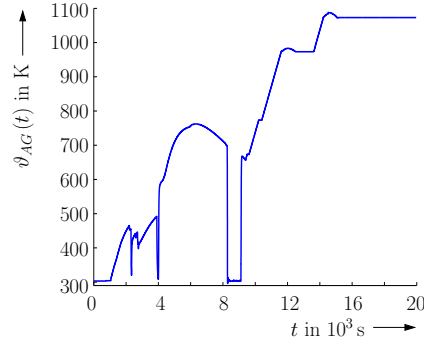
(a) Measured anode gas temperature.
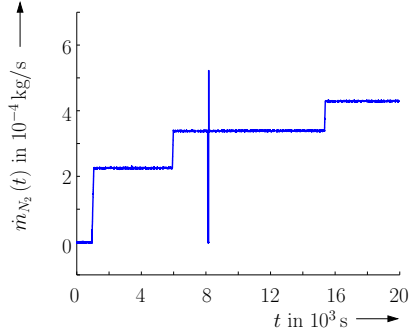
(b) Measured nitrogen mass flow $\dot{m}_{N_2}$.
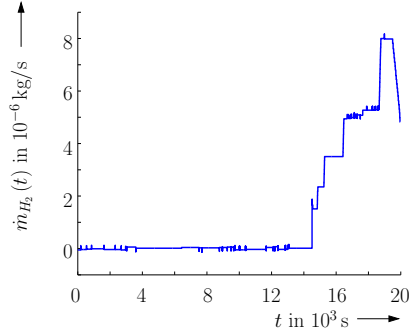
(c) Measured hydrogen mass flow $\dot{m}_{H_2}$.

Figure 7: Measured data of anode gas temperature and mass flows of the anode gas components, where the spike in $\dot{m}_{N_2}$ around $t = 8\cdot10^3\,$s represents an outlier in the measurement.

The cost function for the fundamental sensitivity-based control design is given by

$$\mathcal{D} = \kappa_1 \cdot (\theta_{FC} - \vartheta_{nom})^2 + \kappa_2 \cdot (\dot{m}_{CG} - \dot{m}_{CG,nom})^2 + \kappa_3 \cdot (\vartheta_{CG} - \vartheta_{CG,nom})^2 \quad (37)$$

with the parameters $\kappa_1 = 10^{-3}$, $\kappa_2 = 1$, $\kappa_3 = 1$. Here, the term θ_{FC} denotes the average fuel cell temperature (evaluated for the predicted temperature intervals at each point of time t_μ) according to

$$\theta_{FC} = \frac{1}{M} \sum_{i=1}^{M} \vartheta_{1,i,1} \ . \quad (38)$$

Moreover, the values $\dot{m}_{CG,nom} = 0.003\,\frac{\text{kg}}{\text{s}}$ and $\vartheta_{CG,nom} = 850\,\text{K}$ specify the desired set-points for the SOFC system. As shown in the left column of Fig. 8, the sensitivity-based control procedure does not prevent overshoots of the maximum admissible stack temperature $\vartheta_{max} = 880\,\text{K}$ without further adjustments (case A).

To prevent the overshoots from arising, the cost function (37) has been replaced by

$$\mathcal{D} = (\vartheta_{max} - \min\{\vartheta_{max} - \vartheta_{1,i^*,1}\})^2 \tag{39}$$

with

$$i^* = \underset{i=1,\ldots,M}{\arg\max}\{\sup[\vartheta_{1,i,1}]\} \tag{40}$$

for the complete prediction horizon if a possible overshoot is detected for at least one point of time in $[t_\nu\,;\,t_{\nu+N_p}]$. Here, a quadratic error measure replaces the basic criterion that has been used for the illustrative example in Sec. 2. The reason for this modification is that small overshoots over ϑ_{max} can be tolerated, while larger ones have to be penalized severely since they might be especially harmful to the system. According to Fig. 8, this extension (case B) successfully prevents overshoots for the simple global SOFC model.

Fig. 9 gives a summary of the corresponding simulation results that can be achieved for a semi-discretization of the SOFC stack into three finite volume elements. Also in this scenario, a large overshoot over the maximum admissible temperature ϑ_{max} can be observed in case A. This can be avoided in case B if the extended criterion (39) is used to penalize the resulting violation of the predefined state constraint. However, the preheater temperature for the cathode gas reaches its minimum value (corresponding to the ambient temperature) as soon as one of the stack temperatures reaches the upper bound ϑ_{max}. This conservative behavior can be avoided by the two extensions shown in Fig. 10.
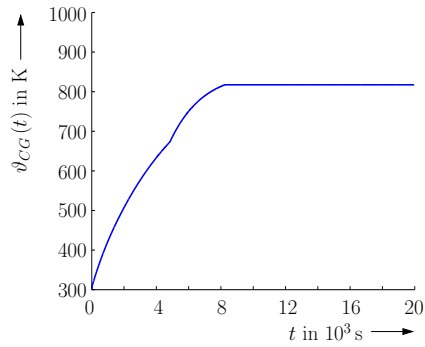
In the left part of Fig. 10, the cost function (37) has been replaced with

$$\mathcal{D} = \kappa_1 \cdot (\theta_{FC} - \vartheta_{nom})^2 + \kappa_2 \cdot \frac{1}{M-1}\sum_{i=1}^{M}(\vartheta_{1,i,1} - \theta_{FC})^2$$
$$+ \kappa_3 \cdot (\dot{m}_{CG} - \dot{m}_{CG,nom})^2 + \kappa_4 \cdot (\vartheta_{CG} - \vartheta_{CG,nom})^2 \quad, \tag{41}$$

where the free parameters are chosen as $\kappa_1 = 10^{-3}$, $\kappa_2 = 1$, $\kappa_3 = 1$, $\kappa_4 = 10$. This extension also takes into account spatial variations of the temperature in the interior of the SOFC stack module. These variations can be counteracted by a suitably large value κ_2. Moreover, the weighting factor for the deviation of the cathode gas temperature from its predefined set-point has been increased as compared to the previous cases. Additionally, the energy-related criterion for reduction of overestimation is now activated. The combination of all of these measures leads to preventing significant overshoots over ϑ_{max} and simultaneously avoids the problem that ϑ_{CG} falls down to its minimum value as soon as the maximum admissible cell temperature is reached.

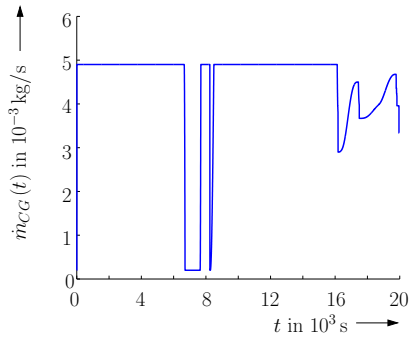As as final extension, the modified cost function

$$\mathcal{D} = \kappa_1 \cdot (\theta_{FC} - \vartheta_{nom})^2 + \kappa_2 \cdot \frac{1}{M-1}\sum_{i=1}^{M}(\vartheta_{1,i,1} - \theta_{FC})^2$$
$$+ \kappa_3 \cdot (\dot{m}_{CG} - \dot{m}_{CG,nom})^2 + \kappa_4 \cdot (\vartheta_{CG} - \vartheta_{CG,nom})^2$$
$$+ \kappa_5 \cdot \left(\exp\left(\beta \cdot \left(-\theta_{FC} + \vartheta_{FC}^-\right)\right) + \exp\left(\beta \cdot \left(\theta_{FC} - \vartheta_{FC}^+\right)\right)\right) \tag{42}$$
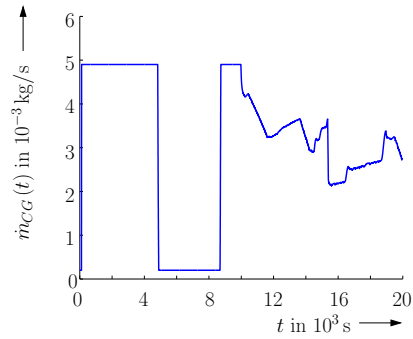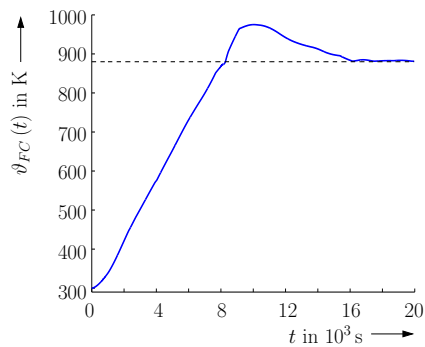
(a) Cathode gas temperature (case A).
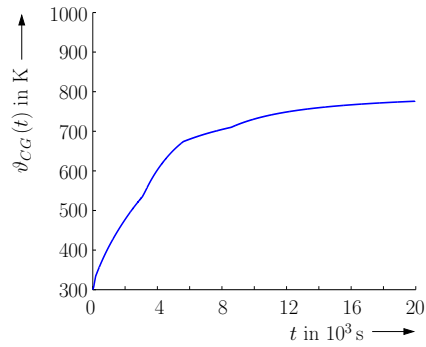
(b) Cathode gas temperature (case B).

(c) Cathode gas mass flow (case A).

(d) Cathode gas mass flow (case B).

(e) Fuel cell temperature (case A).

(f) Fuel cell temperature (case B).

Figure 8: Simulation of the predictive control procedure for $L = 1$, $M = 1$, $N = 1$ without overshoot prevention (case A) and with overshoot prevention (case B).

(a) Cathode gas temperature (case A).

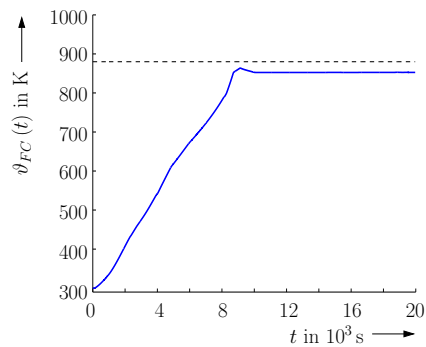(b) Cathode gas temperature (case B).

(c) Cathode gas mass flow (case A).

(d) Cathode gas mass flow (case B).

(e) Fuel cell temperature (case A).

(f) Fuel cell temperature (case B).
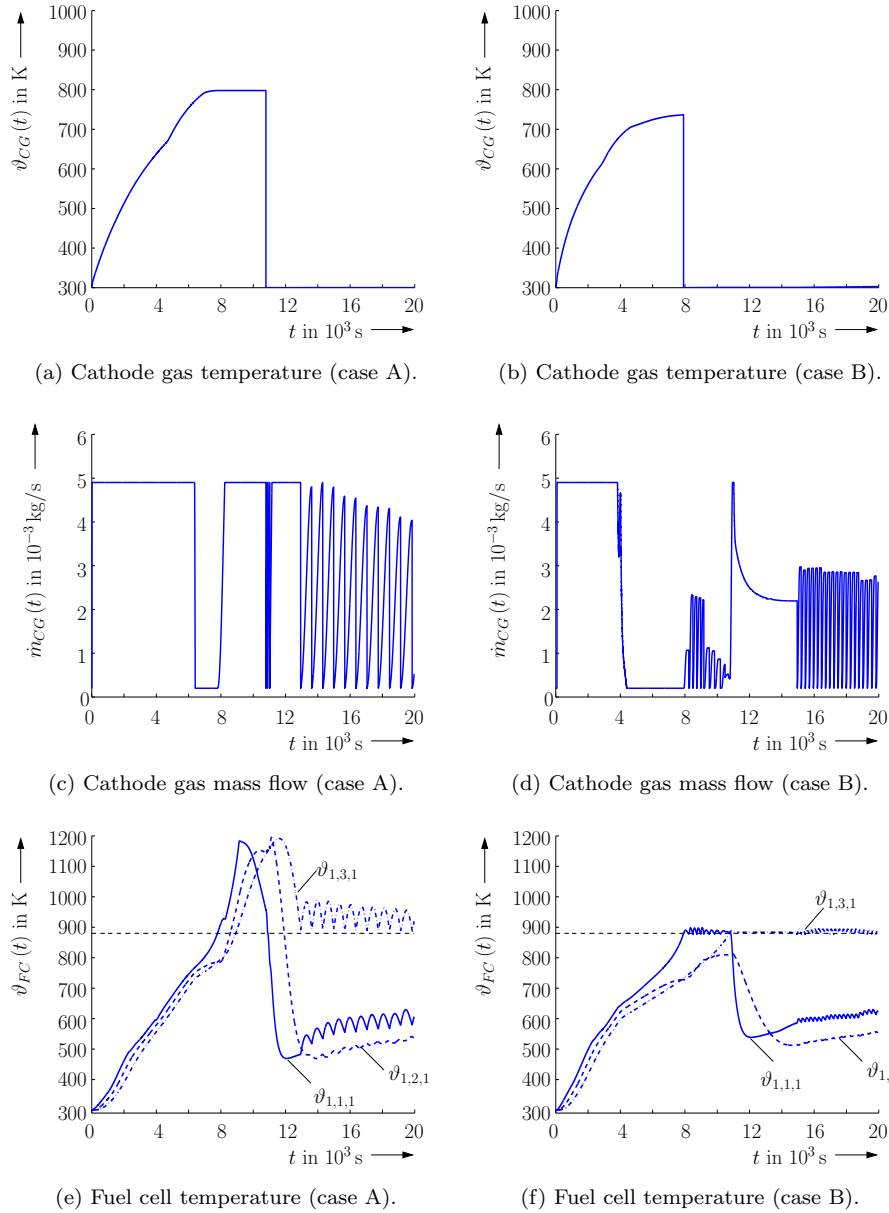
Figure 9: Simulation of the predictive control procedure for $L = 1$, $M = 3$, $N = 1$ without overshoot prevention (case A) and with overshoot prevention, but without the energy-based overestimation reduction (case B).

with $\kappa_1 = 10^{-3}$, $\kappa_2 = 1$, $\kappa_3 = 1$, $\kappa_4 = 10$, $\kappa_5 = 1$, $\beta = 0.02$, $\vartheta_{FC}^- = 820\,\mathrm{K}$, and $\vartheta_{FC}^+ = 880\,\mathrm{K}$ has been studied in the right part of Fig. 10. It shows a similar behavior as the previous result. However, the advantage of this cost function is that it not only penalizes overshoots over the admissible maximum cell temperature ϑ_{FC}^+ but also actively penalizes cell temperatures which are smaller than ϑ_{FC}^-. The simulations without prevention of overshoots have been evaluated with the step size control factor $\alpha_i = 0.001$, while $\alpha_i = 0.002$ is used in the case that the overshoot prevention was active (see also the end of Sec. 2).

4.2 Analysis of Convergence Properties

Concerning the analysis of the applicability of the predictive control strategy on the boundary of the admissible operating range, the reader is referred to the discussion in [14, Sec. 3.2.4, pp. 51, 52]. The corresponding criteria can easily be checked within the current implementation of the interval-based predictive control procedure since the required partial derivatives of the temperature value at the boundary of the admissible operating range are computed anyway by algorithmic differentiation in the presented procedure for overshoot prevention.

4.3 Experimental Validation of the Trajectory Tracking Control Procedure

In Fig. 11, experimental results for the tracking of a desired temperature profile of the SOFC stack module are summarized. Here, the performance criterion

$$
\begin{aligned}
\mathcal{D} = {}& \kappa_1 \cdot \Theta_{FC}^2 + \kappa_2 \cdot \Delta\vartheta_{FC}^2 + \kappa_3 \cdot (\dot{m}_{CG} - \dot{m}_{CG,d})^2 \\
& + \kappa_4 \cdot (\vartheta_{CG} - \vartheta_{FC,d})^2 + \kappa_5 \cdot \Delta\dot{m}_{CG}^2 + \kappa_6 \cdot \Delta\vartheta_{CG}^2
\end{aligned}
\tag{43}
$$

with the tracking error $\Theta_{FC} = \vartheta_{FC,d} - \vartheta_{FC}$, the desired stack temperature $\vartheta_{FC,d}$, a representative mass flow $\dot{m}_{CG,d}$, the spatial variance $\Delta\vartheta_{FC}^2$ of the stack module temperatures $\vartheta_{i,j,k}$ (simplifying to zero in the case $L = 1$, $M = 1$, $N = 1$), and $\Delta\tilde{\mathbf{u}}_\nu = [\Delta\dot{m}_{CG} \ \ \Delta\vartheta_{CG}]^T$ has been used to implement a robust tracking controller for the model with a single lumped temperature value ϑ_{FC}.

A suitable choice of the weighting factors leads to quite smooth control inputs (Figs. 11b and 11c). The resulting control errors in Fig. 11d (thin line around zero) for $t \in [4,000 \,;\, 13,000]\,\mathrm{s}$ are caused by the dynamics of the preheaters which are currently not explicitly accounted for in the control design. On the one hand, the preheater reaches its saturation value during this time interval. On the other hand, it can also be noted that the commanded value for the preheater temperature (solid line in Fig. 11b) changes its value significantly faster than the actual value (dashed line). Hence, future work will deal with an extension of the system model by ODEs which describe this lag behavior of the gas preheaters [26, 23].

5 Conclusions and Outlook on Future Work

In this paper, a framework for the design of sensitivity-based open-loop and closed-loop control strategies has been presented. Representative simulations and experimental results show the applicability of these design procedures to real-life scenarios. In these
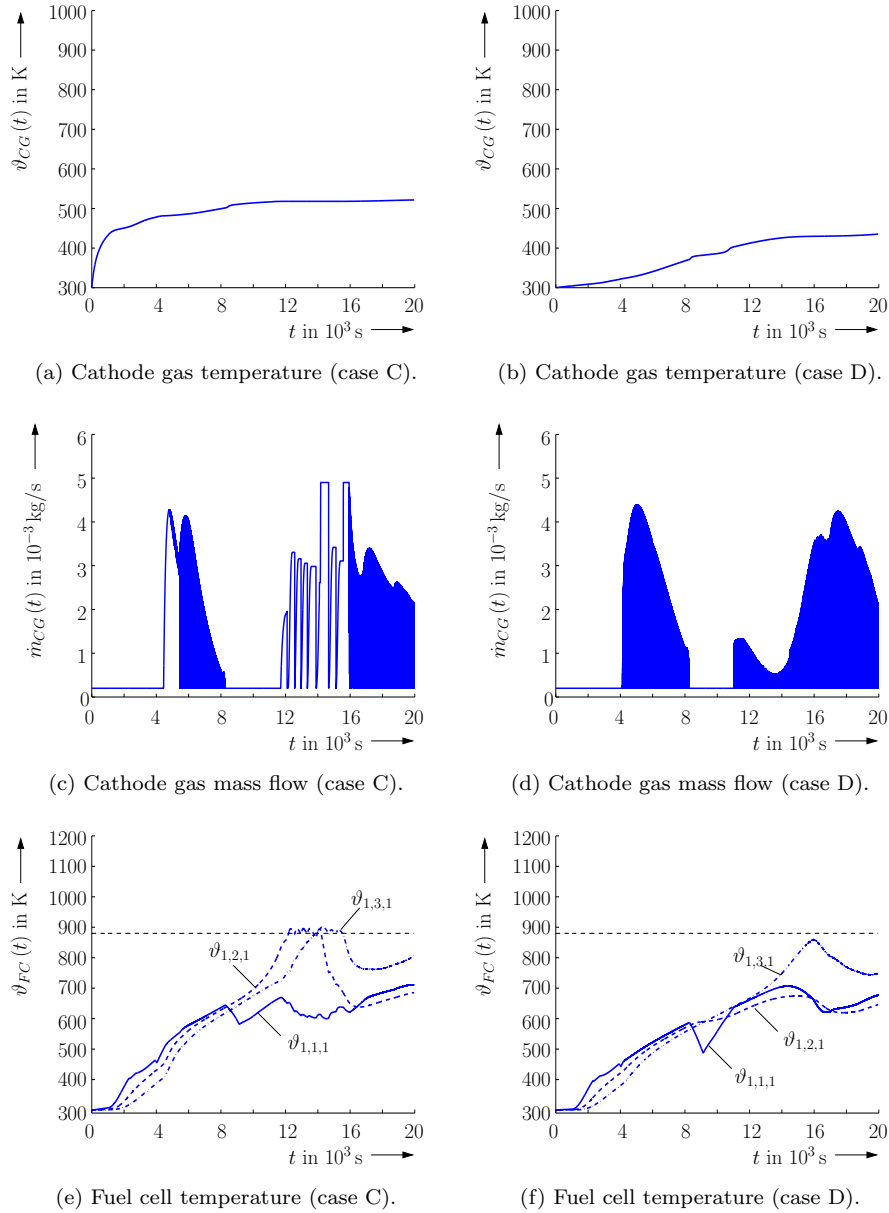
(a) Cathode gas temperature (case C).

(b) Cathode gas temperature (case D).

(c) Cathode gas mass flow (case C).

(d) Cathode gas mass flow (case D).

(e) Fuel cell temperature (case C).

(f) Fuel cell temperature (case D).

Figure 10: Simulation of the predictive control procedure for $L = 1$, $M = 3$, $N = 1$ with overshoot prevention and energy-based overestimation reduction (case C: extended cost function (41), and case D: cost function (42)).
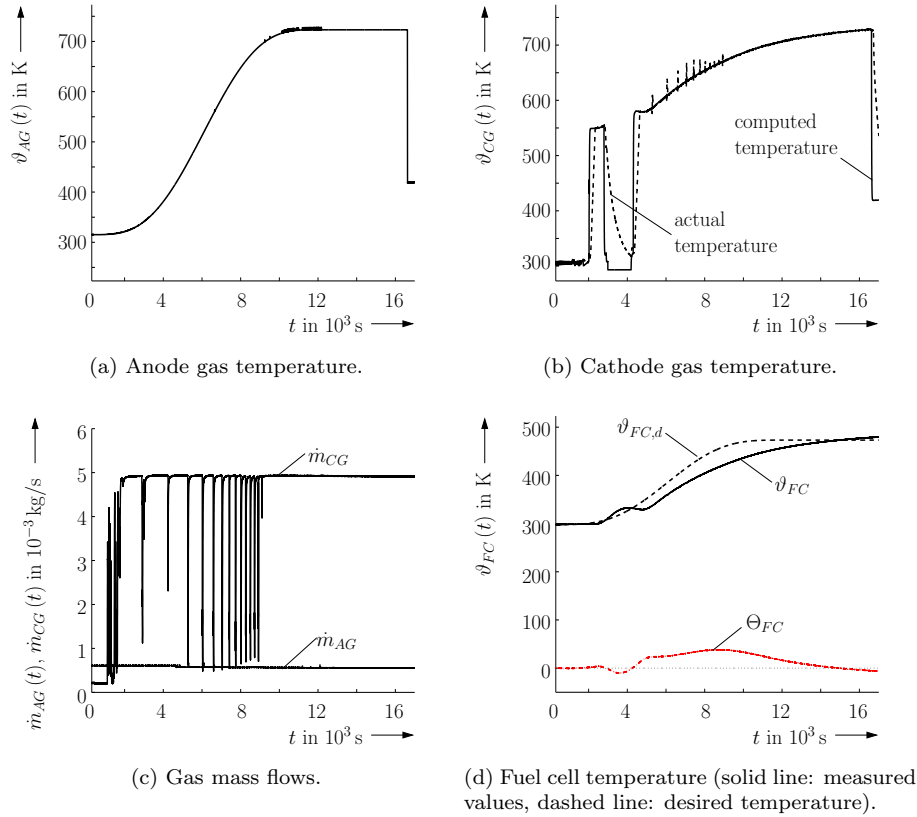
(a) Anode gas temperature.

(b) Cathode gas temperature.

(c) Gas mass flows.

(d) Fuel cell temperature (solid line: measured values, dashed line: desired temperature).

Figure 11: Experimental validation of the predictive controller for $L = 1$, $M = 1$, $N = 1$.

cases, either disturbances have to be compensated in the neighborhood of steady-state operating conditions or the major objective is trajectory tracking.

The main advantage of the presented techniques is their capability to handle uncertainties in system parameters and measured as well as estimated state variables in a straightforward manner. In such a way, it becomes possible to develop approaches which guarantee the compliance of controllers with state and input constraints. As a typical example, the guaranteed prevention of overshooting predefined trajectories has been presented in this paper. Besides an illustrative example of an uncertain linear second-order system (which can be interpreted as a simplified model for the longitudinal dynamics of a vehicle), the design of control strategies for solid oxide fuel cell systems has been considered. These systems typically are described by nonlinear state equations with more than twenty uncertain parameters.

Future work will deal with a generalization of the presented control techniques in a framework using interval analysis for the implementation of sensitivity-based model-predictive control algorithms. Besides the automatic choice of suitable cost functions and the inclusion of Newton-like optimization procedures [22], extensions will be taken

into consideration which allow for the design of state and disturbance estimators. Note that the estimation task is dual to the control of uncertain dynamic systems. For both control and state estimation, possibilities for a guaranteed analysis of the asymptotic stability of the resulting procedures will be investigated. Finally, sensitivity-based approaches also seem to be promising to design gain scheduling methods for other types of nonlinear controllers such as, for example, robust sliding mode control for systems with interval uncertainty.

References

[1] E. Auer, S. Kiel, and A. Rauh. Verified Parameter Identification for Solid Oxide Fuel Cells. In *Proc. of 5th Intl. Conference on Reliable Engineering Computing*, pages 41–55, Brno, Czech Repulic, 2012. available at `http://rec2012.fce.vutbr.cz/documents/proceedings/REC2012_proceedings.p%df`.

[2] C. Bendsten and O. Stauning. FADBAD++, Version 2.1, 2007. `http://www.fadbad.com`.

[3] R. Bove and S. Ubertini, editors. *Modeling Solid Oxide Fuel Cells*. Springer, Berlin, 2008.

[4] Y. Cao. A Formulation of Nonlinear Model Predictive Control Using Automatic Differentiation. *Journal of Process Control*, 15:851–858, 2005.

[5] Y. Cao and W.-H. Chen. Automatic Differentiation Based Nonlinear Model Predictive Control of Satellites Using Magneto-Torquers. In *Proc. of IEEE Conf. on Industrial Electronics and Applications, ICIEA 2009*, pages 913–918, Xi'an, China, 2009.

[6] T. Dötschel, E. Auer, A. Rauh, and H. Aschemann. Thermal Behavior of High-Temperature Fuel Cells: Reliable Parameter Identification and Interval-Based Sliding Mode Control. *Soft Computing*, 17(8):1329–1343, 2013.

[7] T. Dötschel, A. Rauh, L. Senkel, and H. Aschemann. Experimental Validation of Interval-Based Sliding Mode Control for Solid Oxide Fuel Cell Systems. In *Proc. of the European Control Conference ECC 2013*, pages 2489–2494, Zurich, Switzerland, 2013.

[8] M. Fliess, J. Lévine, P. Martin, and P. Rouchon. Flatness and Defect of Nonlinear Systems: Introductory Theory and Examples. *International Journal of Control*, 61:1327–1361, 1995.

[9] A. Griewank and A. Walther. *Evaluating Derivatives: Principles and Techniques of Algorithmic Differentiation*. SIAM, Philadelphia, 2008.

[10] A. Gubner. Non-Isothermal and Dynamic SOFC Voltage-Current Behavior. In S. C. Singhal and J. Mizusaki, editors, *Solid Oxide Fuel Cells IX (SOFC-IX): Volume 1 — Cells, Stacks, and Systems*, pages 814–826. The Electrochemical Society, 2005.

[11] L. Jaulin, M. Kieffer, O. Didrit, and É. Walter. *Applied Interval Analysis*. Springer–Verlag, London, 2001.

[12] M. Kletting and F. Antritter. Robustness Comparison of Tracking Controllers Using Verified Integration. In A. Rauh and E. Auer, editors, *Modeling, Design, and Simulation of Systems with Uncertainties*, Mathematical Engineering, pages 95–115. Springer, 2011.

[13] J.T. Pukrushpan, A.G. Stefanopoulou, and H. Peng. *Control of Fuel Cell Power Systems: Principles, Modeling, Analysis and Feedback Design.* Springer, Berlin, 2nd edition, 2005.

[14] A. Rauh and H. Aschemann. Structural Analysis for the Design of Reliable Controllers and State Estimators for Continuous-Time Dynamical Systems with Uncertainties. In A. Rauh and E. Auer, editors, *Modeling, Design, and Simulation of Systems with Uncertainties*, Mathematical Engineering, pages 43–68. Springer, 2011.

[15] A. Rauh and H. Aschemann. Interval-Based Sliding Mode Control and State Estimation for Uncertain Systems. In *CD-Proc. of IEEE Intl. Conference on Methods and Models in Automation and Robotics MMAR 2012*, Miedzyzdroje, Poland, 2012.

[16] A. Rauh and H. Aschemann. Parameter Identification and Observer-Based Control for Distributed Heating Systems – The Basis for Temperature Control of Solid Oxide Fuel Cells. *Mathematical and Computer Modelling of Dynamical Systems*, 18(4):329–353, 2012.

[17] A. Rauh and H. Aschemann. Sensitivity-Based State and Parameter Estimation for Lithium-Ion Battery Systems. In *Proc. of Intl. Conference System Identification and Control Problems SICPRO'12*, Moscow, Russia, 2012. ISBN 978-5-91450-098-3.

[18] A. Rauh, T. Dötschel, and H. Aschemann. Experimental Parameter Identification for a Control-Oriented Model of the Thermal Behavior of High-Temperature Fuel Cells. In *CD-Proc. of IEEE Intl. Conference on Methods and Models in Automation and Robotics MMAR 2011*, Miedzyzdroje, Poland, 2011.

[19] A. Rauh, T. Dötschel, E. Auer, and H. Aschemann. Interval Methods for Control-Oriented Modeling of the Thermal Behavior of High-Temperature Fuel Cell Stacks. In *Proc. of 16th IFAC Symposium on System Identification SysID 2012*, pages 446–451, Brussels, Belgium, 2012.

[20] A. Rauh, J. Kersten, E. Auer, and H. Aschemann. Sensitivity Analysis for Reliable Feedforward and Feedback Control of Dynamical Systems with Uncertainties. In *Proc. of 8th Intl. Conference on Structural Dynamics EURODYN 2011*, Leuven, Belgium, 2011.

[21] A. Rauh, J. Kersten, E. Auer, and H. Aschemann. Sensitivity-Based Feedforward and Feedback Control for Uncertain Systems. *Computing*, (2–4):357–367, 2012.

[22] A. Rauh, L. Senkel, and H. Aschemann. Sensitivity-Based State and Parameter Estimation for Fuel Cell Systems. In *Proc. of 7th IFAC Symposium on Robust Control Design*, pages 57–62, Aalborg, Denmark, 2012.

[23] A. Rauh, L. Senkel, and H. Aschemann. Design and Experimental Validation of Control Strategies for Commercial Gas Preheating Systems. In *CD-Proc. of IEEE Intl. Conference on Methods and Models in Automation and Robotics MMAR 2013*, Miedzyzdroje, Poland, 2013.

[24] A. Rauh, L. Senkel, T. Dötschel, E. Auer, and H. Aschemann. Numerical Verification and Experimental Validation of Sliding Mode Control for Uncertain Thermal SOFC Models. In *Proc. of the 15th GAMM-IMACS International Symposium on Scientific Computing, Computer Arithmetic, and Validated Numerics SCAN 2012, Special Issue of Reliable Computing*, volume 19, pages 330–350, Novosibirsk, Russia, 2013.

[25] A. Rauh, L. Senkel, J. Kersten, and H. Aschemann. Verified Stability Analysis for Interval-Based Sliding Mode and Predictive Control Procedures with Applications to High-Temperature Fuel Cell Systems. In *Proc. of 9th IFAC Symposium on Nonlinear Control Systems*, pages 570–575, Toulouse, France, 2013.

[26] L. Senkel, A. Rauh, and H. Aschemann. Experimental Validation of a Sensitivity-Based Observer for Solid Oxide Fuel Cell Systems. In *CD-Proc. of IEEE Intl. Conference on Methods and Models in Automation and Robotics MMAR 2013*, Miedzyzdroje, Poland, 2013.

[27] B.J. Spivey, J.D. Hedengren, and T.F. Edgar. Constrained Control and Optimization of Tubular Solid Oxide Fuel Cells for Extending Cell Lifetime. In *Proc. of the American Control Conference ACC 2012*, pages 1356–1361, Montréal, Canada, 2012.

[28] Ch. Stiller. *Design, Operation and Control Modelling of SOFC/GT Hybrid Systems*. PhD thesis, University of Trondheim, 2006.

[29] Ch. Stiller, B. Thorud, O. Bolland, R. Kandepu, and L. Imsland. Control Strategy for a Solid Oxide Fuel Cell and Gas Turbine Hybrid System. *Journal of Power Sources*, 158:303–315, 2006.

[30] V.I. Utkin. *Sliding Modes in Control and Optimization*. Springer–Verlag, Berlin, Heidelberg, 1992.

[31] V.I. Utkin. Sliding Mode Control Design Principles and Applications to Electric Drives. *IEEE Transactions on Industrial Electronics*, 40(1):23–36, 1993.